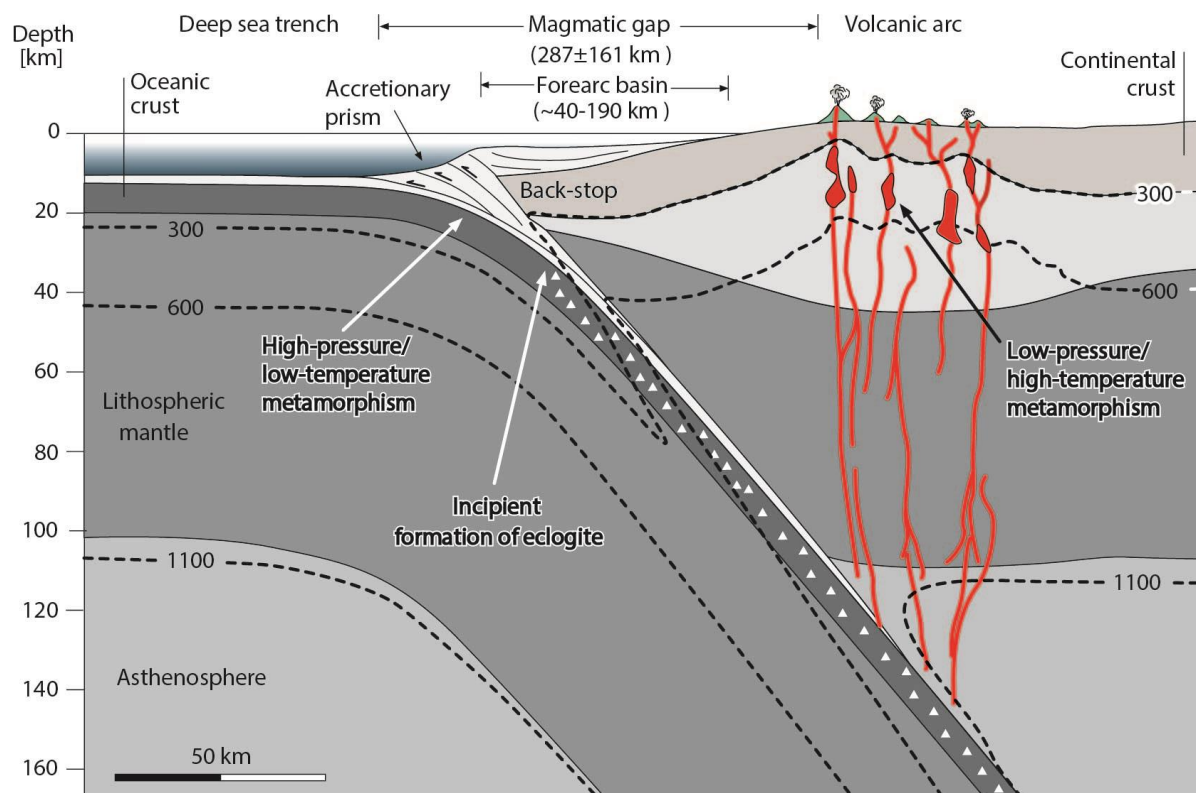




28 Consolidation of the plate tectonic theory in the late 1960s provided a coherent framework for this  
 29 idea, where paired metamorphic belts were explained as a direct result of the subduction process  
 30 (Oxburgh and Turcotte, 1970; Ernst, 1971; Miyashiro, 1972; 1973). This was quantitatively  
 31 demonstrated by the modeling of Oxburgh and Turcotte (1971), which showed that the oceanic  
 32 plate subduction depresses the geotherm near the trench generating low-temperature/high-pressure  
 33 metamorphism, which is preserved in the accretionary prism, and elevates the geotherm in the arc  
 34 region causing high-temperature/low-pressure metamorphism (Fig. 1). Most recent studies have  
 35 expanded this concept to collisional margins and included additional causes in subduction settings  
 36 such as mid-ocean ridge-trench interactions and tectonic juxtaposition of laterally contemporaneous  
 37 metamorphic belts (e.g., Brown, 1998a;b; 2009; 2010; Iwamori, 2000; Maruyama *et al.*, 2010).

38 Early studies in southern Central Chile highlighted similarities between the metamorphic  
 39 zoning of late Paleozoic rocks in the Andean Coastal Cordillera and those described in Japan by  
 40 Miyashiro (1961). In that region, a parallel and coeval arrangement of contrasting geological units  
 41 was interpreted as a subduction-related high-pressure/low-temperature metamorphism to the west  
 42 and a volcanic arc-related low-pressure/high-temperature metamorphism to the east that developed  
 43 along the southwestern Gondwana margin (González-Bonorino and Aguirre, 1970; González-  
 44 Bonorino, 1971; Aguirre *et al.*, 1972). In the last fifty years, numerous studies have supported the  
 45 Pacific-type subduction hypothesis for the origin of the paired metamorphic belt in the Coastal  
 46 Cordillera (Hervé *et al.*, 1974; 1984; 2013; Hervé, 1988; Kato and Godoy 1995; Duhart *et al.*, 2001;  
 47 Glodny *et al.* 2005; 2008; Willner, 2005; Willner *et al.* 2005; Richter *et al.* 2007; Hyppolito *et al.*,  
 48 2014a,b; 2015; Sigoña, 2016; Muñoz-Montecinos *et al.*, 2020).



49 *Figure 1. Cross section through an active continental margin (modified from Frisch et al. 2010)*  
50 *showing the approximate thermal structure in normal subduction settings, main areas of the*  
51 *subduction system, and zones with contrasting metamorphism (Schubert and Turcotte, 1975).*  
52 *Average arc-trench gap is from the Earthbyte group's website*  
53 *(<https://www.earthbyte.org/calculating-arc-trench-distances-using-the-smithsonian-global>*  
54 *[volcanism-project-database/](https://www.earthbyte.org/calculating-arc-trench-distances-using-the-smithsonian-global)) and forearc basin width range is from Noda (2016).*

---

56 In this contribution, I first provide a synthesis of the advances in the study of these  
57 metamorphic rocks and the Coastal Batholith (Fig. 2). Then, I discuss key field-based observations,  
58 along with geochemical and geochronological data from the contemporaneous granitoids, and  
59 contrast these data with our current understanding of the anatomy and dynamics of subduction  
60 zones. This analysis highlights major inconsistencies in the Pacific-type subduction hypothesis for  
61 the origin of the paired metamorphic belt of the Coastal Cordillera and suggests a more complex  
62 late Paleozoic geodynamic setting than previously acknowledged.

63

## 64 **2. Paired metamorphic belt of the Coastal Cordillera in southern Central Chile**

65 Subduction complexes of Late Paleozoic and Mesozoic ages form a lengthy chain of >2000 km  
66 extending from 32°-54°S that developed along the southwestern margin of Gondwana (Hervé,  
67 1988). This revision deals with the basement rocks in the Coastal Cordillera of South Central Chile,  
68 which extends between 32°S and 42°S, and is mostly concentrated on metasedimentary and igneous  
69 units north of the Lanalhue fault zone (~39°S), where these form a contemporaneous paired  
70 metamorphic belt (Fig. 2a). This area holds well-preserved outcrops of a late Carboniferous-Early  
71 Permian metamorphic complex to the west and a contemporaneous batholith to the east jointly  
72 interpreted as recording early subduction stages beneath southwest Gondwana (González-Bonorino  
73 1970, 1971; González-Bonorino y Aguirre 1970; Aguirre *et al.* 1972; Hervé 1977; 1988; Hervé *et*  
74 *al.* 1974; 1984; 2003; 2013; Mpodozis and Ramos; 1989; Beck *et al.*, 1991; Martin *et al.*, 1991;  
75 Kato and Godoy 1995; Duhart *et al.*, 2001; Willner 2005; Willner *et al.* 2004; 2005; 2008; Glodny  
76 *et al.* 2005; 2006; 2008) (Fig. 2a,b). In the following subsections, I summarize the main  
77 characteristics of this igneous-metamorphic belt. In this synthesis, I focus on the most general  
78 aspects of this belt, which are profound enough to highlight arguable aspects of the geodynamic  
79 model proposed so far. In-depth details on metamorphic complexes and igneous rocks can be found  
80 in the references provided in the text.

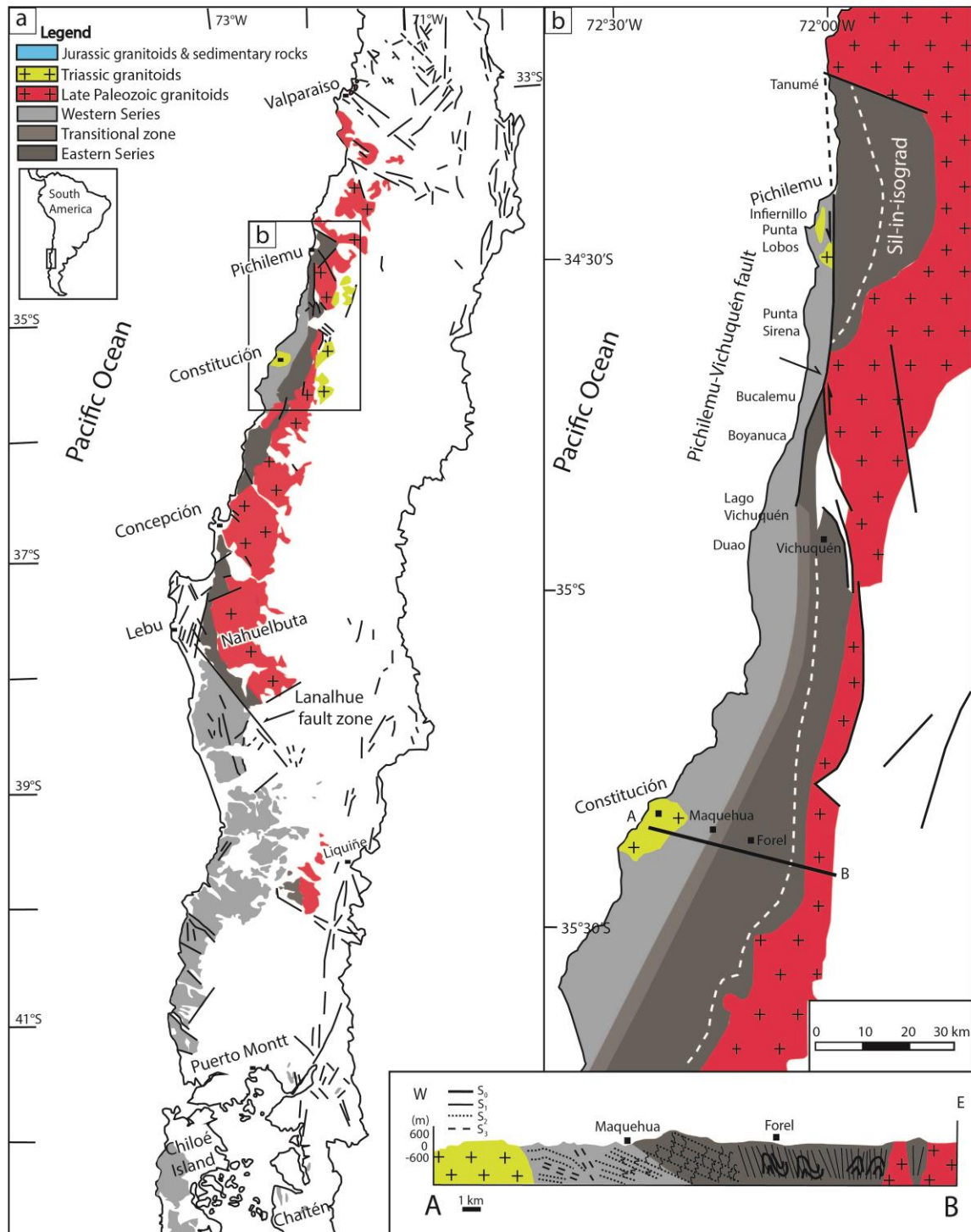
81

## 82            **2.1 Paired metamorphic belt of southern Central Chile**

83            The pioneering studies in the late Paleozoic basement rocks of Coastal Cordillera of southern  
84 Central Chile by González-Bonorino and Aguirre (1970) and González-Bonorino (1971) identified  
85 the Pichilemu, Curepto, and Nirivilo metamorphic facies series that depict a progressive appearance  
86 of mineral zones and facies formed under diverse pressure, temperature, and tectonic regimes. The  
87 metamorphic complex was later divided by Aguirre *et al.* (1972) into the Western and the Eastern  
88 Series (Fig. 2a). The former are intensely deformed oceanic-derived high-pressure/low-temperature  
89 units with sedimentary and basaltic protoliths of abyssal and trench environments, whereas the latter  
90 are associated with less deformed trench-to-forearc metasedimentary rocks of very-low grade  
91 overprinted by low-pressure/high-temperature metamorphism (González-Bonorino, 1971; Aguirre  
92 *et al.*, 1972; Hervé *et al.*, 1984; Hervé, 1988; Willner, 2005; Hyppolito *et al.*, 2014a,b; 2015).

93            The late Paleozoic convergent stage that gave place to this accretionary complex was  
94 preceded by a short-lived Devonian–early Carboniferous passive margin setting (~400–340 Ma,  
95 Willner *et al.*, 2008, 2011 or 420–370 Ma, Hervé *et al.*, 2013) that changed to a convergent margin  
96 with eastward polarity after ~340 Ma. Multi-method geochronological and structural studies  
97 indicate that the accretionary prism would have grown from ~320 to ~224 Ma through frontal  
98 accretion in the Eastern Series and basal accretion in the Western series with W and SW vergence  
99 (Lohrmann, 2002; Glodny *et al.*, 2005; Willner *et al.*, 2005; Richter *et al.*, 2007) (Fig. 3). However,  
100 Richter *et al.* (2007) suggested that the deepest portion of the Eastern Series was also affected by  
101 basal accretion. Field-based analyses indicate that the nature of the contact between the Western  
102 and Eastern Series is regionally variable, changing locally from transitional to tectonic (González-  
103 Bonorino, 1971; Davidson *et al.*, 1987; Richter *et al.*, 2007; Willner *et al.*, 2009; Glodny *et al.*,  
104 2008) (Fig. 2b). Maximum depositional ages obtained from detrital zircon dating in the  
105 metasediments indicate early and late Carboniferous ages for the Eastern and Western series,  
106 respectively, with a provenance from older Gondwana margin basement of the Pampean (~530–510  
107 Ma) and Famatinian (~470 Ma) belts, including reworked cratonic material, and Carboniferous  
108 magmatism east of the present-day Andes (Duhart *et al.*, 2001; Willner *et al.*, 2008; Hervé *et al.*,  
109 2013). However, south of the Lanalhue fault zone Permian maximum depositional ages have been  
110 documented in the Western Series with detritus derived from the Choiyoi province (~287–245 Ma)  
111 or subvolcanic plutonic rocks in the North Patagonian massif (~290–260 Ma) (Hervé *et al.*, 2013).  
112 The Western Series is formed by schists and phyllites that contain metre- to kilometre-sized slices  
113 of metabasites of high-pressure greenschists, epidote and garnet amphibolites, and blueschists  
114 (Kato, 1985; Hervé, 1988; Shira *et al.*, 1990; Kato and Godoy 1995; Willner *et al.* 2004; Willner

115 2005; Hyppolito *et al.*, 2014a). The latter (~9.5–11 kbar, and 350–385°C) are scarce and the record  
 116 of high-pressure conditions is given by greenschists that bear Na–



117  
 118 *Figure 2. a) Geological sketch map of the studied area (34–42°S) showing the late Paleozoic*  
 119 *metamorphic complexes and late Paleozoic and Triassic granitoids from the Coastal Batholith.*

120 *Figure modified from Hervé et al. (2013). b) Geological map of the Coastal Cordillera at Pichilemu*  
121 *and Constitución regions (34°-35°40'S) with cross section A-B. Figure modified from Willner et al.*  
122 *(2009).*

---

123 Ca amphibole and phengite (~7–9.3 kbar, and 380–420°C) and indicate a subduction-related  
124 metamorphic gradient in the range of ~11–16 °C/km (Willner, 2005). Local occurrences of garnet-  
125 bearing mica schists in the Punta Sirena region record the highest temperature conditions  
126 (retrograde conditions in the range 9.6–14.7 kbar and 390–440°C, at ~320 Ma) and a counter-  
127 clockwise P–T path (Willner, 2005) (Fig. 2b). Zircon dating of accreted sediments and <sup>40</sup>Ar–<sup>39</sup>Ar  
128 cooling ages in phengite from high-pressure greenschists from the Western Series indicates that  
129 basal accretion began at ~308 Ma (Willner *et al.*, 2005, 2008; 2009, 2012; Hyppolito *et al.*, 2014b)  
130 (Fig. 3). As demonstrated by Hyppolito *et al.* (2015), basal accretion preceded both the peak of  
131 blueschist metamorphism at ~300 Ma in the Pichilemu region (Willner *et al.*, 2005) and cooling of  
132 the Eastern Series in the interval 301–292 Ma (Fig. 3). During the evolution of the accretionary  
133 complex these rocks reached depths of 10–50 km, and were later exhumed at variable rates ranging  
134 from 0.03–2.0 mm/year (Willner *et al.*, 2004; Willner, 2005; Willner *et al.*, 2005; Kato *et al.*, 2008;  
135 Hyppolito *et al.*, 2014b). Geochemical and isotopic studies indicate that metabasites from the  
136 Western Series are ocean-derived tholeiitic and alkali basalts, with N-MORB, E-MORB, and OIB  
137 signatures (Kato, 1985; Hervé, 1988; Kato & Godoy, 1995; Schira *et al.*, 1990; Hyppolito *et al.*,  
138 2014a). These metabasites are interpreted as formed in an oceanic basin setting characterized by  
139 shallow and deep mantle sources, such as plume-influenced mid-ocean ridge (Hyppolito *et al.*,  
140 2014a).

141 The Eastern Series is formed by psammo-pelitic sequences associated with early  
142 Carboniferous trench and Devonian passive margin sedimentary deposits that preserve bedding and  
143 sedimentary structures (e.g., Hervé, 1988; Willner, 2005; Glodny *et al.*, 2008). The Eastern Series is  
144 classically understood as the rear part of the late Paleozoic accretionary wedge, reflecting a position  
145 transitional to the backstop area (Hervé, 1988; Willner *et al.*, 2000; Glodny *et al.*, 2008) (Fig. 4).  
146 During the development of the accretionary wedge, the Eastern Series was intruded by late  
147 Paleozoic granitoids belonging to the Coastal Batholith causing a metamorphic overprinting at 3  
148 kbar (296–301 Ma, <sup>40</sup>Ar/<sup>39</sup>Ar muscovite plateau ages, Willner *et al.*, 2005) of the very low-grade  
149 frontal accretion-related metamorphism (Willner *et al.*, 2005; Glodny *et al.*, 2008; Hervé *et al.*,  
150 2013; Deckart *et al.*, 2014) (Fig. 2a,b). Metamorphism in the Eastern Series records increasing  
151 metamorphic grade from west to east, from greenschist to amphibolite and locally granulite facies  
152 conditions and thermobarometric studies indicate high-temperature/low-pressure metamorphic  
153 conditions in the range of 720–400°C and 2.5–3.5 kbar (Aguirre *et al.* 1972; Hervé, 1977; Willner

154 2005; Willner et al., 2005; Hyppolito et al., 2015). According to Hyppolito *et al.* (2015), the thermal  
155 overprint occurred after the frontal accretion-related deformation (D1) and likely before or early  
156 during the development of a penetrative foliation (S2) (Fig. 3). A contemporaneous paired  
157 metamorphic belt in southern Central Chile has been corroborated by the age range for the high-  
158 temperature metamorphism in the Eastern Series that falls into the time span determined for the  
159 peak of high-pressure metamorphism in the Western Series at 292–320 Ma (Willner *et al.* 2005;  
160 Hyppolito *et al.*, 2015) (Fig. 3).

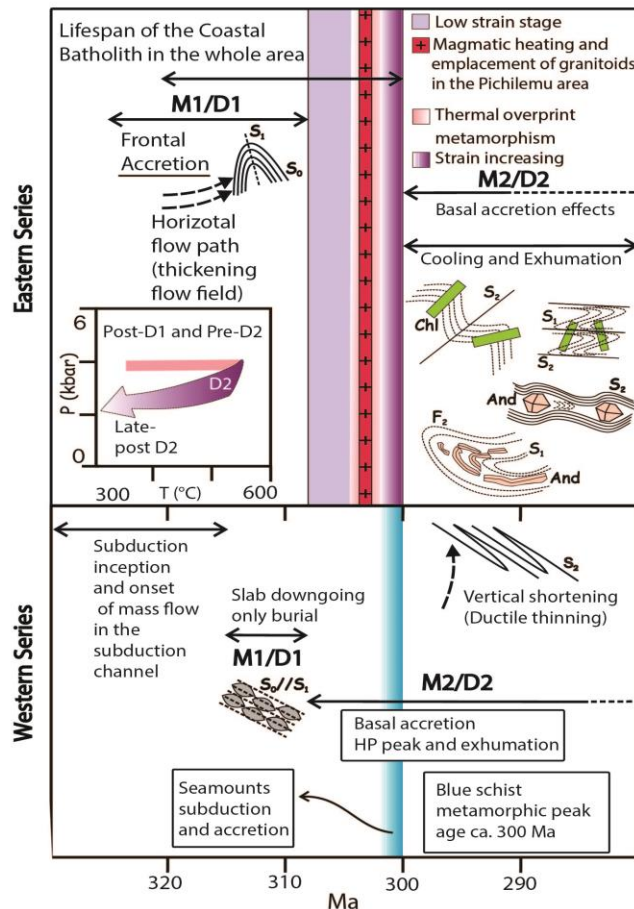
161

### 162 **3.2 The Coastal Batholith of south Central Chile**

163 The Coastal Batholith crops out between 33°S and 38°20'S along the Coastal Cordillera,  
164 and is dislocated to the east by the Lanalhue strike-slip fault at 40°S (Glodney *et al.*, 2008) (Fig.  
165 2a). This is a large composite calc-alkaline igneous body of meta- to peraluminous composition  
166 mostly made of tonalite, granodiorites, and granite with minor diorite that intruded syn- and post-  
167 tectonically metamorphic rocks of the Eastern series (Cordani *et al.*, 1976; Hervé *et al.*, 1988; 2013;  
168 Parada, 1999; Parada *et al.*, 1999; 2007; Charrier *et al.*, 2015). More locally, equivalent mafic rocks  
169 have also been described intruding in basally accreted rocks of the Choapa Metamorphic Complex  
170 (~318 Ma, Sigoña, 2016). Radiometric ages obtained in previous studies along the length of the  
171 batholith yielded Late Carboniferous (Pennsylvanian) ages, mostly between ~300 and 320 Ma,  
172 indicating a short-lived magmatic event (K-Ar, Cordani *et al.*, 1976; Rb-Sr isochron ages, Shibata *et*  
173 *al.*, 1984; U-Pb zircon ages, Godoy and Loske, 1988; Rb-Sr isochron and K-Ar ages, Hervé *et al.*,  
174 1988; K/Ar and  $^{40}\text{Ar}/^{39}\text{Ar}$ , Beck *et al.*, 1991, K-Ar ages, Martin *et al.* 1991; U-Pb zircon ages, Gana  
175 and Tosdal, 1996; Rb-Sr isochron, Lucassen *et al.*, 2004; two-point Rb-Sr ages, Glodny *et al.*, 2008;  
176 U-Pb zircon ages, Pineda and Calderón, 2008; U-Pb SHRIMP zircon ages, Deckart *et al.*, 2014).  
177 As mentioned in the previous subsection, the intrusion of this large igneous body is responsible for  
178 the metamorphic overprint at around 300 Ma on the eastern side of Eastern Series (e.g., Willner *et*  
179 *al.*, 2005; Hyppolito *et al.*, 2015) (Figs. 2b and 3). Also, ages for the metamorphic peaks on the  
180 basally accreted Western Series indicate that metamorphism overlapped with the intrusion of the  
181 Coastal Batholith (Willner et al., 2005; Hervé *et al.* 2013) (Fig. 3).

182 Based on the analysis of Carboniferous mafic enclaves Parada *et al.* (1999) noted that in  
183 terms of Y, La, and Nb, these have geochemical signatures of continental basalts derived from an  
184 enriched lithospheric mantle. These authors indicated that the Sr–Nd isotope data (Initial  $^{87}\text{Sr}/^{86}\text{Sr}$  =  
185 0.7057 - 0.7098 and  $\epsilon\text{Nd}$  = -2 - -4) suggest that these mafic rocks were derived from primary  
186 enriched mantle-derived magmas. Lucassen *et al.* (2004) also found enriched isotopic compositions  
187 in the late Paleozoic Nahuelbuta granitoids presenting initial  $^{87}\text{Sr}/^{86}\text{Sr}$  ratios between 0.705 and

188 0.715 and  $\epsilon\text{Nd}$  values between -2.5 and -7.5 (Fig. 2a). These authors noted that the REE patterns in  
 189 late Paleozoic rocks of the Coastal Batholith are similar to those of the metamorphic accretionary  
 190 basement and an average upper continental crust that together, with their isotopic composition,  
 191 indicate a crustal origin. Recently, Deckart *et al.* (2014) showed that Lu-Hf isotopic analyses on  
 192 zircon grains with ages between ~320 and 300 Ma have initial  $\epsilon\text{Hf}(i)$  values from +1.67 - -5.64,  
 193 with most of the analyses between +1 and -4 epsilon units and the  $T_{\text{DM2}}$  in these rocks suggest  
 194 Mesoproterozoic crustal residence ages. These authors also presented  $\delta_{18}\text{O}$  ratios from the dated  
 195 zircon grains ranging from 6.4 - 8.6‰ with a prominent group with values between 6.0 and 7.5‰  
 196 and a minor group between 8.0 and 9.0‰. According to Deckart *et al.* (2014), these data indicate  
 197 that the magmas were likely derived from crustal sources with a prominent sedimentary input as  
 198 suggested by the elevated  $\delta_{18}\text{O}$  values. However, as pointed out by these authors, a mantle input  
 199 cannot be completely ruled out. Therefore, geochemical and isotopic data suggest that the Coastal  
 200 Batholith has a high proportion of reworked old crustal material, indicating that either the magmas  
 201 assimilated large amounts of metasediments from Eastern Series, which represent reworked old  
 202 continental crust, and/or that the Eastern Series was partly underlain by an old continental back-stop  
 203 basement (Parada *et al.*, 1999; Lucassen *et al.*, 2004; Glodny *et al.*, 2006; Deckart *et al.*, 2014).



205 *Figure 3. Image depicting the temporal relations between deformation in Western and Eastern*  
206 *series, and the overall evolution of the accretionary wedge in the Pichilemu region. Figure modified*  
207 *from Hyppolito et al. (2015). See text for discussion.*

---

208

209 The geodynamic context of the Coastal Batholith is classically interpreted as a subduction  
210 setting where this igneous body represents part of the large southwestern Gondwana magmatic arc  
211 (Hervé *et al.*, 1988; Parada, 1990; Parada *et al.*, 1999; 2007; Lucassen *et al.*, 2004; Charrier *et al.*,  
212 2007; 2015; Deckart *et al.*, 2014; del Rey *et al.*, 2016; Oliveros *et al.*, 2020; among others).  
213 According to the regional analysis of Charrier *et al.* (2015), differences in peak metamorphic ages  
214 in accretionary complexes north of 33°S and the contrasting ages of igneous rocks south and north  
215 of this latitude likely indicates a major segmentation in the ancient convergent margin.

216

### 217 **3. Discussion: A circum-Pacific Miyashiro-type or a forearc paired metamorphic belt in** 218 **south Central Chile?**

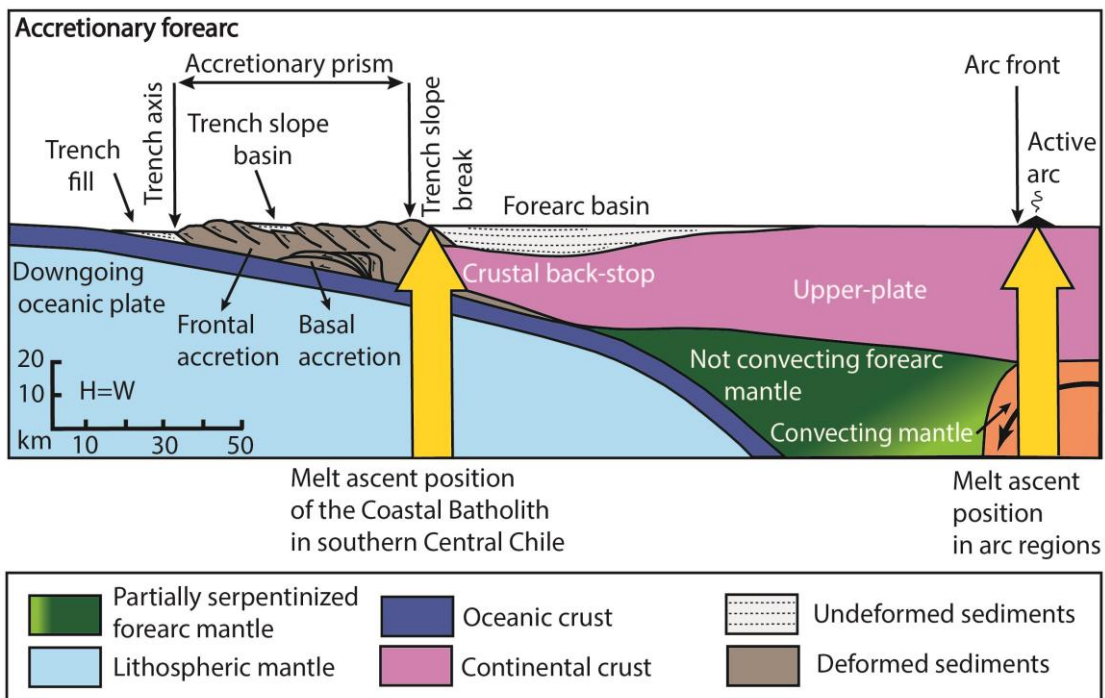
219 The hypothesis of a circum-Pacific Miyashiro-type paired metamorphic belt for the origin of the  
220 late Paleozoic igneous-metamorphic complexes of south Central Chile has remained unquestioned  
221 since its proposal in the seventies (González-Bonorino and Aguirre, 1970; González-Bonorino,  
222 1971; Aguirre *et al.*, 1972; Hervé *et al.*, 1974, 1984, 2013; Hervé, 1988; Kato, 1985; Kato and  
223 Godoy 1995; Duhart *et al.*, 2001; Glodny *et al.* 2005; 2008; Willner 2005; Willner *et al.* 2005;  
224 Richter *et al.* 2007; Hyppolito *et al.*, 2014a,b; 2015; Muñoz-Montecinos *et al.*, 2020). Below I argue  
225 that field relations between the metamorphic and igneous units, and possibly the time and  
226 geochemistry of the Coastal Batholith, highlight inconsistencies in this model and are not  
227 compatible with our current understanding of typical subduction zones.

228 The geological configuration of subduction zones indicates that the contemporaneous arc and  
229 accretionary prism systems do not overlap and that both develop under contrasting geothermal  
230 gradients, which constitute the foundations of Miyashiro's concept of paired metamorphic belts  
231 (e.g., Oxburgh and Turcotte, 1971; Stern, 2002) (Fig. 1). Global analyses of active subduction  
232 zones indicate that average arc-trench gaps are  $287 \pm 161$  km (<https://www.earthbyte.org/calculating-arc-trench-distances-using-the-smithsonian-global-volcanism-project-database/>) and the rear areas  
233 of accretionary prisms are commonly separated from arc regions by ~40-190 km wide forearc  
234 basins (Noda, 2016) (Figs. 1 and 4). Notably, this distance could be larger if forearc fold-and thrust  
235 belts are present as recently recognized in some areas of the Andes (e.g., Armijo *et al.* 2015;  
236 Riesner *et al.*, 2018; Martinez *et al.*, 2020; Encinas *et al.*, 2020). Volcanic arcs and accretionary  
237

238 prisms do not superpose even in subduction settings with the highest known slab angles, such as  
239 Mariana-type subduction zones with up to 90° dipping slabs (Uyeda and Kanamori, 1979). An  
240 apparent superposition of these two systems is possible when subsequent tectonic processes, such as  
241 strike-slip or forearc underthrusting, juxtapose the geological record of both areas (e.g., Brown *et*  
242 *al.*, 1998a,b; 2010). In the case of the igneous-metamorphic complexes in the Coastal Cordillera  
243 between 33°S and 42°S, a tectonic superposition of both belts is ruled out by field relations, and  
244 despite subsequent deformation during Andean orogeny, an in-situ formation has been  
245 demonstrated (e.g., Willner *et al.*, 2005). Detailed mapping in the last decades has confirmed early  
246 observations on the intrusive nature of the contact between the Coastal Batholith and the Eastern  
247 Series, and established a transitional contact between the latter and the Western Series at several  
248 latitudes (González-Bonorino, 1971; Davidson *et al.*, 1987; Richter *et al.*, 2007; Willner *et al.*,  
249 2009) (Fig. 2b). Also, Sigoña (2016) documented ~318 Ma mafic dykes associated with the Coastal  
250 Batholith intruding high-pressure/low-temperature rocks at 31°30'S. The latter observations  
251 constitute a challenge for the interpretation of a circum-Pacific-type paired metamorphic belt for  
252 late Paleozoic rocks in this area. The fact that throughout the development of the accretionary  
253 wedge, the frontally accreted Eastern Series was intruded by the partially contemporaneous Coastal  
254 Batholith (~320-300 Ma) (Willner *et al.*, 2005; Hervé *et al.*, 2013, 2014; Deckart *et al.*, 2014),  
255 indicate a geodynamic setting that departs substantially from typical subduction zones (Fig. 4). In  
256 the latter, magmatic activity is usually concentrated several kilometers away from the accretionary  
257 prisms and is developed above a mantle wedge (e.g., Stern, 2002; Tatsumi, 2005; Gerya and  
258 Meilick, 2011) (Figs. 1 and 4). A major implication of the proximity of the igneous activity to the  
259 paleo-trench is that the proposed magmatic arc nature of the Coastal Batholith is untenable (e.g.,  
260 Hervé, 1988; Parada, 1990; Parada *et al.*, 1999; 2007; Lucassen *et al.*, 2004; Deckart *et al.*, 2014;  
261 Sigoña, 2016). The abnormal character of the Coastal Batholith is not only limited to the  
262 conspicuous emplacement site within the overall subduction system (Fig. 4). Deckart *et al.* (2014)  
263 already highlighted that the short period of time of batholith emplacement (~20 Ma) and the  
264 petrogenetic features indicating a major source from the accretionary prism metasediments and/or  
265 the back-stop lithosphere (Parada, 1990; Parada *et al.*, 1999; Lucassen *et al.*, 2004) contrast those of  
266 typical cordilleran batholiths. The latter, are commonly formed along tens or hundred million years  
267 through multiple pulses of magmatism with variable mantle wedge and crust inputs depending,  
268 among other parameters, on the upper-plate nature and thickness (e.g., Ducea *et al.*, 2015). Indeed,  
269 these key observations have been integrated in evolutionary models of most recent studies at these  
270 latitudes depicting a magmatic activity to the east that intrudes the frontally accreted Eastern series  
271 and interacts with a potential back-stop lithosphere during magma ascent (e.g., Glodney *et al.*, 2008;

272 Hyppolito et al., 2014b; Díaz-Alvarado *et al.*, 2019). However, the geodynamic meaning of such an  
 273 unusual geological configuration has been overlooked so far, and a continental arc setting was  
 274 suggested in the latter and subsequent studies as well (e.g., del Rey *et al.*, 2016; Oliveros *et al.*,  
 275 2020).

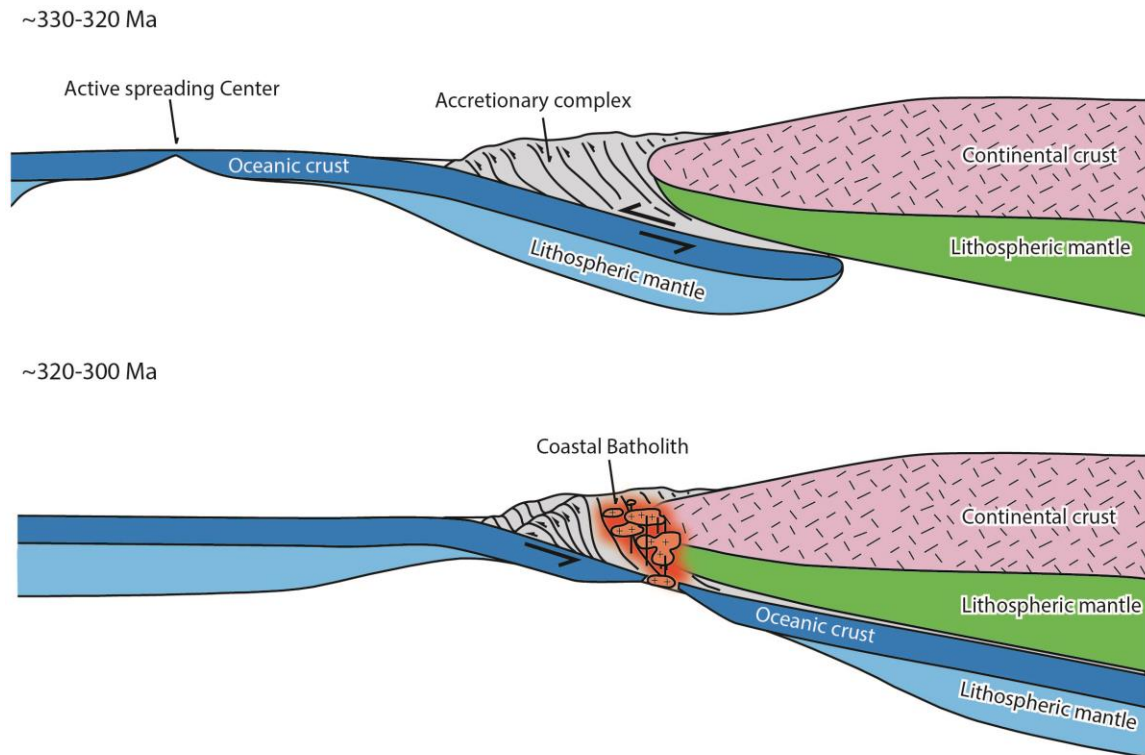
276 According to Willner *et al.* (2004; 2005), deep transport of a considerable volume of sediments  
 277 below the upper mantle wedge during subduction initiation could have provided hydrous fluids  
 278 triggering fluid-flux mantle melting and magmatism at the earliest stage in the evolution of the  
 279 paired metamorphic belt. However, the latter cannot effectively explain the mainly crustal-like  
 280 sources in the Coastal Batholith (Parada, 1990; Parada *et al.*, 1999; Lucassen *et al.*, 2004; Deckart  
 281 *et al.*, 2014). Alternatively, Deckart *et al.* (2014) proposed that deeply subducted sediments could  
 282 have been melted at mantle depths, which is compatible with isotopic values of the Coastal  
 283 Batholith. Nevertheless, in either case, deep sediment subduction up to the mantle wedge within a  
 284 shallow subduction setting, as inferred at the onset of convergence in this region (Willner *et al.*,  
 285 2004), would have still triggered magmatism far from the accretionary prism. The latter is also  
 286 confirmed by 2-D numerical modeling studies where buoyant plumes of partially melted sediments  
 287 in the mantle wedge ascend several kilometers away from accretionary prisms impacting beneath  
 288 the arc and backarc areas, even at normal slab angles (30-45°) (Gerya and Yuen, 2003; Gerya and  
 289 Meilick, 2011)



291 *Figure 4. Cross-section at scale of an accretionary forearc (modified after Stern, 2002). This image*  
292 *illustrates the unusual setting where the Coastal Batholith of southern Central Chile was emplaced*  
293 *during the late Paleozoic.*

---

294 In order to trigger substantial magmatic activity in the overall cold forearc region, a thermal  
295 anomaly is needed below the rear part of the late Paleozoic accretionary prism. Although not  
296 common in normal subduction zones, forearc magmatism and related high-temperature/low-  
297 pressure metamorphism have been documented in recent and ancient convergent settings in  
298 association with asthenosphere upwelling produced by the development of slab gaps (e.g., Uyeda  
299 and Miyashiro, 1974; Marshak and Karig, 1977; DeLong and Fox, 1979; Iwamori, 2000;  
300 Wakabayashi, 2004; Santosh and Kusky, 2010; see Gianni and Perez-Luján, 2021, for a recent  
301 synthesis). Slab windows or gaps are openings in the downgoing plate that allow hot sub-slab  
302 asthenosphere to flow through the slab hole impacting beneath the upper-plate margin. This  
303 phenomena influences the arc and backarc magmatism (e.g., Abratis, and Wörner, G., 2001;  
304 Rosenbaun *et al.*, 2008; Thorkelson *et al.*, 2011), the upper-plate thermal structure (Roche *et al.*,  
305 2018; Ávila and Dávila, 2018), the mantle flow in subduction zones, and the overall plate  
306 kinematics (Guillaume *et al.*, 2010; Király *et al.*, 2020). Slab gap development can be produced by  
307 several processes but mostly results from two general causes. One is the presence of buoyancy  
308 anomalies in the downgoing plate such as oceanic plateaus, aseismic ridges, or continental  
309 fragments (e.g., Cloos, 1993) that resist subduction and lead to slab ruptures. The latter could be  
310 caused by local slab necking forming holes within the downgoing plate (e.g., Király *et al.*, 2020),  
311 vertical slab tearing (e.g., Rosenbaun *et al.*, 2008), or by propagation of horizontal tears (e.g.,  
312 Wortel and Spakman, 2000). The other cause of slab gap development comprises the divergence or  
313 reactivation and separation of a preexisting plate discontinuity such as the separation of an active  
314 spreading center during subduction (Uyeda and Miyashiro, 1974; DeLong and Fox, 1979; Marshak  
315 and Karig, 1977; Dickinson and Snyder, 1979) or a major fault onboard the oceanic plate such as  
316 fracture zones and transform faults (e.g., Pesicek *et al.*, 2012). Although most of the processes  
317 forming slab gaps induce more or less similar magmatic and thermal effects in the upper-plate, mid-  
318 ocean ridge subduction is characterized by a substantial impact on the forearc area. In that region,  
319 ridge subduction may cause uplift and unconformity development, local ophiolites emplacement,  
320 near-trench MORB (Mid-Ocean-Ridge-Basalt) intrusions, felsic magmatism by crustal anatexis of  
321 the accretionary prism (*blow-torch effect*, DeLong *et al.*, 1979), and low-pressure/high-temperature  
322 metamorphism (Marshak and Karig, 1977; DeLong *et al.*, 1979; Nelson *et al.*, 1993; Underwood *et al.*,  
323 1993; see Sisson *et al.*, 2003, for a synthesis). In this context, heating and melting of the  
324 accretionary prism can take place with or without cessation of subduction (Underwood *et al.*, 1993;



325

326 *Figure 5. Conceptual model of a forearc paired metamorphic belt for the origin of the igneous-*  
 327 *metamorphic complexes of the Coastal Cordillera of southern Central Chile (33°-40°S (modified*  
 328 *from Wakabayashi, 2004).*

329

330 Brown, 1998b; Iwamori, 2000). Subduction of a trench-parallel mid-ocean ridge segment could be a  
 331 possible explanation for the short-lived thermal anomaly (~20 Ma) beneath the rear part of the late  
 332 Paleozoic accretionary prism and the formation of the Coastal Batholith (Fig. 5). According to the  
 333 2-D numerical modeling of Iwamori (2000) initial mid-ocean ridge subduction can drive high-  
 334 temperature/low-pressure metamorphism and magmatism before the opening of a slab window  
 335 explaining near-trench granitoids coexisting with paired metamorphic belts. The latter study found  
 336 that ridge crest subduction produces a substantial thermal anomaly that depending on plate  
 337 kinematics can be dissipated in up to 30 Myr after the ridge subduction event. Hence, subduction of  
 338 an active spreading center and possibly the incipient ridge opening during initial subduction could  
 339 have provided the necessary heat and fluids to melt materials from the rear accretionary prism and  
 340 back-stop lithosphere, which is compatible with the isotopic and geochemical signatures of the  
 341 Coastal Batholith (Parada, 1990; Parada *et al.*, 1999; Lucassen *et al.*, 2004; Deckart *et al.*, 2014)  
 342 (Fig. 5). Local occurrences of equivalent forearc magmatic activity along the coast at 28°30-

343 29°30'S described by Creixell *et al.* (2016) likely indicate that a similar process could have taken  
344 place to the north of the study area. Therefore, the igneous-metamorphic rocks of the Coastal  
345 Cordillera of southern Central Chile (33°-42°S) could have been formed as a forearc-type paired  
346 metamorphic belt, whose spatio-temporal relations indicate an origin associated with a near-trench  
347 thermal anomaly (Fig. 5). The short time spanned between the onset of subduction and the forearc  
348 magmatism (~20 Myr), and the apparent lack of an arc region to the east, attesting for subduction  
349 magnitudes below the critical slab dehydration depth ( $120 \pm 40$  km, Tatsumi, 2005) necessary for  
350 fluid flux melting in the mantle wedge, indicate that the ridge would have been located relatively  
351 near the Devonian passive margin of southwest Gondwana (Fig 5).

352

#### 353 **4. Conclusion**

354 A revision of metamorphic rocks and the contemporaneous igneous intrusions along the coast  
355 of southern Central Chile challenges the pioneering hypothesis of a subduction-related Miyashiro-  
356 type paired metamorphic belt for the origin of this igneous-metamorphic complex. The short-lived  
357 intrusion of the Coastal Batholith in the rear area of the partially synchronous accretionary wedge,  
358 and geochemical and isotopic data from the igneous rocks indicating substantial participation of  
359 sources from the accretionary prism and the back-top lithosphere, are not compatible with typical  
360 subduction settings. I suggest that the igneous-metamorphic rocks from the study area formed as a  
361 forearc-type paired metamorphic belt. The latter would have resulted from a near-trench thermal  
362 anomaly triggered by the subduction of a mid-ocean ridge crest in late Paleozoic times.

363

#### 364 **Acknowledgements**

365 G.M.G. recognizes the support received by CONICET and discussion with several members of the  
366 Laboratorio de Tectónica Andina and the Instituto Sismológico Ing. Fernando Volponi (IGSV)  
367 through the years.

368

#### 369 **Declarations of competing interests**

370 The authors declare that they have no known competing financial interests or personal relationships  
371 that could have appeared to influence the work reported in this paper.

372

373 **References**

- 374 Abratis, M., Wörner, G., 2001. Ridge collision, slab-window formation, and the flux of Pacific  
375 asthenosphere into the Caribbean realm. *Geology*, 29(2), 127-130.
- 376 Armijo, R., Lacassin, R., Coudurier-Curveur, A., Carrizo, D., 2015. Coupled tectonic evolution of  
377 Andean orogeny and global climate. *Earth-Science Reviews*, 143, 1-35.
- 378 Aguirre, L., Hervé, F., Godoy, E., 1972. Distribution of metamorphic facies in Chile, an outline.  
379 *Kristalinikum*, Prague, 9, p. 7–19.
- 380 Ávila, P., Dávila, F. M., 2018. Heat flow and lithospheric thickness analysis in the Patagonian  
381 asthenospheric windows, southern South America. *Tectonophysics*, 747, 99-107.
- 382 Beck, M.E. Jr., Garcia, R. A., Burmester, R.F., Munizaga, F., Hervé, F., Drake, R.E., 1991.  
383 Paleomagnetism and geochronology of late Paleozoic granitic rocks from the Lake District of  
384 southern Chile: implications for accretionary tectonics. *Geology*, 19, 332-335.
- 385 Brown, M., 1998a. Unpairing metamorphic belts: P–T paths and a tectonic model for the Ryoke  
386 belt, southwest Japan. *Journal of Metamorphic Geology*, 16, 3–22.
- 387 Brown, M., 1998b. Ridge –trench interactions and high-T–low-P metamorphism, with particular  
388 reference to the cretaceous evolution of the Japanese islands. In: Treloar, P.J., O’Brien, P.J. (Eds.),  
389 *What Drives Metamorphism and Metamorphic Reactions?* Special Publication-Geological Society  
390 of London, vol. 138, pp. 137 – 169.
- 391 Brown, M., 2009. Metamorphic patterns in orogenic systems and the geological record. In:  
392 Cawood, P.A., Kröner, A. (Eds), *Accretionary Orogens in Space and Time*. Geological Society,  
393 London, Special Publications vol. 318, pp. 37–74.
- 394 Brown, M., 2010. Paired metamorphic belts revisited. *Gondwana Research*, 18(1), 46-59.
- 395 Charrier, R., Pinto, L., Rodríguez, M. P., 2007. Tectonostratigraphic evolution of the Andean  
396 Orogen in Chile. In: Moreno, T. & Gibbons, W. (eds) *The Geology of Chile*. Geological Society,  
397 London, 21–114.
- 398 Charrier, R., Ramos, V. A., Tapia, F., Sagripanti, L., 2015. Tectono-stratigraphic evolution of the  
399 Andean Orogen between 31 and 37 S (Chile and Western Argentina). Geological Society, London,  
400 *Special Publications*, 399(1), 13-61.
- 401 Cloos, M., 1993. Lithospheric buoyancy and collisional orogenesis: Subduction of oceanic plateaus,  
402 continental margins, island arcs, spreading ridges, and seamounts. *Geological Society of America*  
403 *Bulletin*, 105(6), 715-737.

404 Cordani, U., Munizaga, F., Hervé, F., Hervé, M., 1976. Edades radiométricas provenientes del  
405 basamento cristalino de la Cordillera de la Costa de las provincias de Valparaíso y Santiago, Chile.  
406 In Congreso Geológico Chileno, No. 1, Actas 2: F213-F221. Santiago.

407 Creixell, C., Oliveros, V., Vásquez, P., Navarro, J., Vallejos, D., Valin, X., Godoy, E., Ducea,  
408 M.N., 2016. Geodynamics of late carboniferous early Permian forearc in north Chile (28°30'-29°30'  
409 S). *Journal of the Geological Society of London*, 173(5), 757–772.

410 Davidson, J., Mpodozis, C., Godoy, E., Hervé, F., Pankhurst, R., Brook, M., 1987. Late Paleozoic  
411 accretionary complexes on the Gondwana margin of southern Chile: Evidence from the Chonos  
412 Archipelago. *Gondwana Six: Structure, Tectonics, and Geophysics*, 40, 221-227.

413 Deckart, K., Hervé, F., Fanning, C.M., Ramírez, V., Calderón, M., Godoy, E., 2014. U-Pb  
414 geochronology and Hf-O isotopes of zircons from the Pennsylvanian Coastal Batholith, South-  
415 Central Chile. *Andean Geology*, 41, 49-82.

416 DeLong, S.E., Schwarz, W.M., Anderson, R.N., 1979. Thermal effects of  
417 ridge subduction. *Earth Planetary Science Letters*, 44, 239–246.

418 Del Rey, A., Deckart, K., Arriagada, C., Martínez, F., 2016. Resolving the paradigm of the late  
419 Paleozoic–Triassic Chilean magmatism: Isotopic approach. *Gondwana Research*, 37, 172-181.

420 Díaz-Alvarado, J., Galaz, G., Oliveros, V., Creixell, C., Calderón, M., 2019. Fragments of the  
421 late Paleozoic accretionary complex in central and northern Chile: similarities and differences as a  
422 key to decipher the complexity of the pre-Andean cycle. A. Folguera, B. Horton (Eds.), *Andean*  
423 *Tectonics*, Elsevier.

424 Dickinson, W.R., and Snyder, W.S., 1979. Geometry of triple junctions related  
425 to San Andreas transform. *Journal of Geophysical Research*, 84, 561–572.

426 Ducea, M. N., Saleeby, J. B., Bergantz, G., 2015. The architecture, chemistry, and evolution of  
427 continental magmatic arcs. *Annual Review of Earth and Planetary Science Letters*, 43, 299-331.

428 Duhart, P., Mc Donough, M., Muñoz, J., Martin, M., Villeneuve, M., 2001. El Complejo  
429 Metamórfico Bahía Mansa en la Cordillera de la Costa del centro-sur de Chile (39°30'–42°S):  
430 geocronología K\Ar, <sup>40</sup>Ar/<sup>39</sup>Ar y U\Pb, implicancias en la evolución del margen sur-occidental de  
431 Gondwana. *Revista Geológica de Chile*, 28, 179–208.

432 Encinas, A., Sagripanti, L., Rodríguez, M. P., Orts, D., Anavalón, A., Giroux, P., Otero, J.,  
433 Echaurren, A., Zambrano, P., Valencia, V., 2020. Tectonosedimentary evolution of the Coastal  
434 Cordillera and Central Depression of south-Central Chile (36° 30'-42° S). *Earth-Science Reviews*,  
435 103465.

436 Ernst, W.G., 1971. Metamorphic zonations on presumably subducted lithospheric plates from  
437 Japan, California and the Alps. *Contributions to Mineralogy and Petrology*, 34, 43–59.

438 Frisch, W., Meschede, M., Blakey, R., 2011. Plate tectonics: continental drift and mountain  
439 building. Springer-Verlag Berlin Heidelberg, pp. 149–158

440 Gana, P., Tosdal, R., 1996. Geocronología U-Pb y K-Ar en intrusivos del Paleozoico y Mesozoico  
441 de la Cordillera de la Costa, Región de Valparaíso, Chile. *Revista Geológica de Chile*, 23 (2), 151-  
442 164.

443 Gerya, T. V., Yuen, D. A., 2003. Rayleigh–Taylor instabilities from hydration and melting propel  
444 ‘cold plumes’ at subduction zones. *Earth and Planetary Science Letters*, 212(1-2), 47-62.

445 Gerya, T. V., Meilick, F. I., 2011. Geodynamic regimes of subduction under an active margin:  
446 effects of rheological weakening by fluids and melts. *Journal of Metamorphic Geology*, 29(1), 7-31.

447 Gianni, G. M., Luján, S. P., 2021. Geodynamic controls on magmatic arc migration and  
448 quiescence. *Earth-Science Reviews*, 103676.

449 Gill, J. B., 1981. *Orogenic andesites and plate tectonics* Springer-Verlag. New York, 390.

450 Glodny, J., Lohrmann, J., Echtler, H., Gräfe, K., Seifert, W., Collao, S., Figueroa, O., 2005. Internal  
451 dynamics of a paleoaccretionary wedge: insights from combined isotope tectonochronology and  
452 sandbox modelling of the South-Central Chilean forearc. *Earth and Planetary Science*  
453 *Letters*, 231(1-2), 23-39.

454 Glodny, J., Echtler, H. et al. 2006. Long-term geological evolution and mass flow balance of the  
455 South- Central Andes. In: Oncken, O., Chong, G., Franz, G., Giese, P., Go'tze, H. J., Ramos, V.,  
456 Strecker, M. & Wigger, P. (eds) *The Andes – Active Subduction Orogeny*. *Frontiers in Earth*  
457 *Sciences*, Springer, Berlin, 1, 401–442.

458 Glodny, J., Echtler, H., Collao, S., Ardiles, M., Burón, P., Figueroa, O., 2008. Differential late  
459 paleozoic active margin evolution in South-Central Chile (37° S–40° S)–the Iñalhue fault  
460 zone. *Journal of South American Earth Sciences*, 26(4), 397-411.

461 González-Bonorino, F., 1970. Series metamórficas del basamento cristalino de la Cordillera de la  
462 Costa de Chile Central. *Departamento de Geología, Universidad de Chile. Publicaciones*, 37, 1–68.

463 González-Bonorino, F., 1971. Metamorphism of the crystalline basement of central Chile. *Journal*  
464 *of Petrology*, 12(1), 149-175.

465 González-Bonorino, F., Aguirre, L., 1970. Metamorphic facies series of the crystalline basement of  
466 Chile. *Geologische Rundschau*, 59(3), 979-994.

467 Guillaume, B., Moroni, M., Funicello, F., Martinod, J., Faccenna, C., 2010. Mantle flow and  
468 dynamic topography associated with slab window opening: Insights from laboratory  
469 models. *Tectonophysics*, 496(1-4), 83-98.

470 Hervé, F., Munizaga, F., Godoy, E., Aguirre, L., 1974. Late Paleozoic K/Ar ages of blueschists  
471 from Pichilemu, central Chile. *Earth and Planetary Science Letters*, 23(2), 261-264.

472 Hervé, F., 1977. Petrology of the crystalline basement of the Nahuelbuta mountains, southcentral  
473 Chile, in: Ishikawa, T., Aguirre L. (Eds). *Comparative studies on the geology of the Circum-Pacific*  
474 *Orogenic Belt in Japan and Chile*. Japan Society for the Promotion of Science, Tokyo, pp. 1-51.

475 Hervé, F., Kawashita, K., Munizaga, F. Bassei, M., 1984. Rb–Sr isotopic ages from late Paleozoic  
476 metamorphic rocks of Central Chile. *Journal of the Geological Society, London*, 141, 877–884.

477 Hervé, F., 1988. Late Paleozoic subduction and accretion in Southern Chile. *Episodes Journal of*  
478 *International Geoscience*, 11(3), 183-188.

479 Hervé, F., Fanning, C.M., Pankhurst, R.J., 2003. Detrital zircon age patterns and provenance in the  
480 metamorphic complexes of Southern Chile. *Journal of South American Earth Sciences*, 16, 107–  
481 123.

482 Hervé, F., Calderón, M., Fanning, C. M., Pankhurst, R. J., Godoy, E., 2013. Provenance variations  
483 in the Late Paleozoic accretionary complex of central Chile as indicated by detrital  
484 zircons. *Gondwana Research*, 23(3), 1122-1135.

485 Hyppolito, T., Juliani, C., García-Casco, A., Meira, V. T., Bustamante, A., Hervé, F., 2014a. The  
486 nature of the Palaeozoic oceanic basin at the southwestern margin of Gondwana and implications  
487 for the origin of the Chilenia terrane (Pichilemu region, central Chile). *International Geology*  
488 *Review*, 56(9), 1097-1121.

489 Hyppolito, T., García-Casco, A., Juliani, C., Meira, V. T., Hall, C., 2014b. Late Paleozoic onset of  
490 subduction and exhumation at the western margin of Gondwana (Chilenia Terrane):  
491 Counterclockwise P–T paths and timing of metamorphism of deep-seated garnet–mica schist and  
492 amphibolite of Punta Sirena, Coastal Accretionary Complex, central Chile (34 S). *Lithos*, 206, 409-  
493 434.

494 Hyppolito, T., Juliani, C., Garcia-Casco, A., Meira, V., Bustamante, A., Hall, C., 2015. LP/HT  
495 metamorphism as a temporal marker of change of deformation style within the Late Palaeozoic  
496 accretionary wedge of central Chile. *Journal of Metamorphic Geology*, 33(9), 1003-1024.

497 Kato, T. T., 1985. Pre-Andean orogenesis in the Coast Ranges of central Chile. *Geological Society  
498 of America Bulletin*, 96(7), 918-924.

499 Iwamori, H., 2000. Thermal effects of ridge subduction and its implications for the origin of  
500 granitic batholith and paired metamorphic belts. *Earth and Planetary Science Letters* 181, 131–144.

501 Kato, T.T., Godoy, E., 1995. Petrogenesis and tectonic significance of Late Paleozoic coarse-  
502 crystalline blueschist and amphibolite boulders in the coastal range of Chile. *International Geology  
503 Review*, 37, 992–1006

504 Kato, T.T., Sharp, W.D., Godoy, E., 2008. Inception of a Devonian subduction zone along the  
505 southwestern Gondwana margin: 40Ar–39Ar dating of eclogite–amphibolite assemblages in  
506 blueschist boulders from the coastal range of Chile (41°S). *Canadian Journal of Earth Sciences*, 45,  
507 337–351.

508 Király, A., Portner, D.E., Haynie, K.L., Chilson-Parks, B.H., Ghosh, T., Jadamec, M., Makushkina,  
509 A., Manga, M., Moresi, L., O`Farrel, K.A., 2020. The effect of slab gaps on subduction dynamics  
510 and mantle upwelling. *Tectonophysics*, 785, 228458.

511 Lucassen, F., Trumbull, R., Franz, G., Creixell, C., Vásquez, P., Romer, R. L., Figueroa, O., 2004.  
512 Distinguishing crustal recycling and juvenile additions at active continental margins: the Paleozoic  
513 to recent compositional evolution of the Chilean Pacific margin (36–41 S). *Journal of South  
514 American Earth Sciences*, 17(2), 103-119.

515 Lohrmann, J., 2002. Identification of parameters controlling the accretive and tectonically erosive  
516 mass-transfer mode at the South-Central and North Chilean forearc using scaled 2D sandbox  
517 experiments, Dissertation, FU Berlin, 2002, Scientific Technical Report STR02/10, [http://www.gfz-  
518 potsdam.de/bib/zbstr.htm](http://www.gfz-potsdam.de/bib/zbstr.htm).

519 Marshak, R. S., Karig, D. E., 1977. Triple junctions as a cause for anomalously near-trench igneous  
520 activity between the trench and volcanic arc. *Geology*, 5(4), 233-236.

521 Maruyama, S., Masago, H., Katayama, I., Iwase, Y., Toriumi, M., Omori, S., 2010. A new  
522 perspective on metamorphism and metamorphic belts. *Gondwana Research*, 18(1), 106-137.

523 Martin, M.W., Kato, T.T., Rodriguez, C., Godoy, E., Duhart, P., McDonough, M., Campos,  
524 A., 1999. Evolution of the late Paleozoic accretionary complex and overlying forearc-magmatic arc,

525 south central Chile (38°-41°S): Constraints for the tectonic setting along the southwestern margin of  
526 Gondwana. *Tectonics*, 18, 582-605.

527 Martínez, F., Kania, J., Muñoz, B., Riquelme, R., López, C., 2020. Geometry and development of a  
528 hybrid thrust belt in an inner forearc setting: Insights from the Potrerillos Belt in the Central Andes,  
529 northern Chile. *Journal of South American Earth Sciences*, 98, 102439.

530 Miyashiro, A., 1961. Evolution of metamorphic belts. *Journal of Petrology*, 2, 277–311.

531 Miyashiro, A., 1972. Metamorphism and related magmatism in plate tectonics. *American Journal of*  
532 *Science*, 272, 629-656.

533 Miyashiro, A., 1973. Paired and unpaired metamorphic belts. *Tectonophysics*, 17(3), 241-254.

534 Muñoz-Montecinos, J., Angiboust, S., Cambeses, A., García-Casco, A., 2020. Multiple veining in a  
535 paleo-accretionary wedge: The metamorphic rock record of prograde dehydration and transient  
536 high pore-fluid pressures along the subduction interface (Western Series, central  
537 Chile). *Geosphere*, 16(3), 765-786.

538 Noda, A., 2016. Forearc basins: Types, geometries, and relationships to subduction zone  
539 dynamics. *Bulletin*, 128(5-6), 879-895.

540 Nelson, E., Forsythe, R., Diemer, J., Allen, M., and Urbina, O., 1993. Taitao ophiolite: A ridge  
541 collision ophiolite in the forearc of southern Chile (46°S). *Revista Geológica de Chile*, 20, 137.

542 Oliveros, V., V´asquez, P., Creixell, C., Lucassen, F., Ducea, M., Ciocca, I., González, J., Espinoza,  
543 M., Salazar, E., Coloma, F., Kasemann, S., 2020. Lithospheric evolution of the pre-and early  
544 andean convergent margin. *Chile Gondwana Research*, 80, 202–227.

545 Oxburgh, E.R., Turcotte, D.L., 1970. Thermal structure of island arcs. *Geological Society of*  
546 *America Bulletin* 81, 1665–1688.

547 Oxburgh, E.R., Turcotte, D.L., 1971. Origin of paired metamorphic belts and crustal dilation in  
548 island arc regions. *Journal of Geophysical Research*, 76, 1,315–1,327.

549 Parada, M.A., 1990. Granitoid plutonism in central Chile and its geodynamic implications; a  
550 review. *Geological Society of America Special Paper*, 241, 51–66.

551 Parada, M.A., López-Escobar, L., Oliveros, V., Fuentes, F., Morata, D., Calderón, M., Aguirre, L.,  
552 Féraud, G., Espinoza, F., Moreno, H., Figueroa, O., Muñoz Ravo, J., Troncoso Vásquez, R., Stern,  
553 C.R., 2007. Andean Magmatism. In ‘The Geology of Chile’ (Moreno, T.; Gibson, W.; editors). The  
554 Geological Society, London, Special Publication 4: 115-146

555 Pesicek, J. D., Engdahl, E. R., Thurber, C. H., DeShon, H. R. Lange, D., 2012. Mantle subducting  
556 slab structure in the region of the 2010 M 8.8 Maule earthquake (30–40 S), Chile. *Geophysical*  
557 *Journal International*, 191(1), 317-324.

558 Pineda, G.; Calderón, M., 2008. Geología del área Monte Patria-El Maqui, Región de Coquimbo.  
559 Servicio Nacional de Geología y Minería, Carta Geológica de Chile, Serie Geología Básica, 116, 44  
560 p., 1 mapa escala 1:100.000.

561 Richter, P., Ring, U., Willner, A. P. Leiss, B. 2007. Structural contacts in subduction complexes and  
562 their tectonic significance: the Late Palaeozoic coastal accretionary wedge of central Chile. *Journal*  
563 *of the Geological Society*, London, 164, 203–14.

564 Riesner, M., Lacassin, R., Simoes, M., Carrizo, D., Armijo, R., 2018. Revisiting the crustal  
565 structure and kinematics of the central Andes at 33.5° S: Implications for the mechanics of Andean  
566 Mountain building. *Tectonics*, 37(5), 1347-1375.

567 Roche, V., Sternai, P., Guillou-Frotier, L., Menant, A., Jolivet, L., Bouchot, V., Gerya, T., 2018.  
568 Emplacement of metamorphic core complexes and associated geothermal systems controlled by  
569 slab dynamics. *Earth and Planetary Science Letters*, 498, 322-333.

570 Rosenbaum, G., Gasparon, M., Lucente, F.P., Peccerillo, A., Miller, M.S., 2008. Kine-matics of  
571 slab tear faults during subduction segmentation and implications for Italian magmatism. *Tectonics*,  
572 27.

573 Santosh, M., Kusky, T., 2010. Origin of paired high pressure–ultrahigh-temperature orogens: a  
574 ridge subduction and slab window model. *Terra Nova*, 22(1), 35-42.

575 Schubert, G., Yuen, D. A., and Turcotte, D. L., 1975. Role of phase transitions in a dynamic mantle.  
576 *Geophysical Journal of the Royal Astronomical Society*, 42, 705–735.

577 Shibata, K., Ishihara, S., Ulriksen, C., 1984. Rb-Sr ages and initial  $^{87}\text{Sr}/^{86}\text{Sr}$  ratios of late Paleozoic  
578 granitic rocks from northern Chile. *Bulletin of the Geological Survey of Japan*, 35 (2), 537-545.

579 Sigoña León, P. A., 2016. Petrología, geocronología e implicancias tectónicas de enclaves  
580 graníticos del paleozoico tardío en un dique mesozoico en el sector costero del Norte Chico (31  
581 30'S), Chile.

582 Sisson, V. B., Pavlis, T. L., Roeske, S. M., Thorkelson, D. J., 2003. Introduction: An overview of  
583 ridge-trench interactions in modern and ancient settings. *Geological Society of America Special*  
584 *Paper*, 371, 1-18.

585 Stern, R. J., 2002. Subduction zones. *Reviews of geophysics*, 40(4), 3-1.

586 Tatsumi, Y., 2005. The subduction factory: How it operates in the evolving Earth. *GSA Today* 15,  
587 4–10.

588 Thorkelson, D. J., Madsen, J. K., Slaggett, C. L., 2011. Mantle flow through the Northern  
589 Cordilleran slab window revealed by volcanic geochemistry. *Geology*, 39(3), 267-270.

590 Underwood, M.B., Byrne, T., Hibbard, J.P., DiTullio, L., Laughland, M.M., 1993. The effects of  
591 ridge subduction on the thermal structure of accretionary prisms: a Tertiary example from the  
592 Shimanto Belt of Japan. In: Underwood, M.B. (Ed.), *Thermal Evolution of the Tertiary Shimanto  
593 Belt, Southwest Japan: An Example of Ridge –trench Interaction*. Special Paper, vol. 273.  
594 Geological Society of America, Boulder, Colorado, pp. 151 – 168.

595 Uyeda, S., Miyashiro, A., 1974. Plate tectonics and the Japanese Islands: a synthesis. *Geological  
596 Society of America Bulletin*, 85(7), 1159-1170.

597 Uyeda, S., Kanamori, H., 1979. Back-arc opening and the mode of subduction. *Journal of Geo-  
598 physical Research, Solid Earth*, 84, 1049–1061.

599 Wakabayashi, J., 2004. Tectonic mechanisms associated with P–T paths of regional metamorphism:  
600 alternatives to single-cycle thrusting and heating. *Tectonophysics*, 392(1-4), 193-218.

601 Willner, A.P., Hervé, F., Massonne, H.J., 2000. Mineral chemistry and pressure-temperature  
602 evolution of two contrasting high-pressure-low-temperature belts in the Chonos archipelago,  
603 Southern Chile. *Journal of Petrology*, 41, 309-330.

604 Willner, A. P., Glodny, J., Gerya, T. V., Godoy, E., Massonne, H. J., 2004. A counterclockwise PTt  
605 path of high-pressure/low-temperature rocks from the Coastal Cordillera accretionary complex of  
606 south-central Chile: constraints for the earliest stage of subduction mass flow. *Lithos*, 75(3-4), 283-  
607 310.

608 Willner, A. P., 2005. Pressure–temperature evolution of a Late Palaeozoic paired metamorphic belt  
609 in North–Central Chile (34°–35° 30' S). *Journal of Petrology*, 46(9), 1805-1833.

610 Willner, A. P., Thomson, S. N., Kröner, A., Wartho, J. A., Wijbrans, J. R., Hervé, F., 2005. Time  
611 markers for the evolution and exhumation history of a Late Palaeozoic paired metamorphic belt in  
612 North–Central Chile (34°–35° 30' S). *Journal of Petrology*, 46(9), 1835-1858.

613 Willner, A. P., Gerdes, A., Massonne, H. J., 2008. History of crustal growth and recycling at the  
614 Pacific convergent margin of South America at latitudes 29–36 S revealed by a U–Pb and Lu–Hf

615 isotope study of detrital zircon from late Paleozoic accretionary systems. *Chemical Geology*, 253(3-  
616 4), 114-129.

617 Willner, A. P., Richter, P. P., Ring, U., 2009. Structural overprint of a late Paleozoic accretionary  
618 system in north-central Chile (34-35°S) during post-accretional deformation. *Andean*  
619 *Geology*, 36(1), 17-36.

620 Willner, A. P., Gerdes, A., Massonne, H. J., Schmidt, A., Sudo, M., Thomson, S. N., Vujovich, G.,  
621 2011. The geodynamics of collision of a microplate (Chilenia) in Devonian times deduced by the  
622 pressure–temperature–time evolution within part of a collisional belt (Guarguaraz Complex, W-  
623 Argentina). *Contributions to Mineralogy and Petrology*, 162(2), 303-327.

624 Wortel, M. J. R., Spakman, W., 2000. Subduction and slab detachment in the Mediterranean-  
625 Carpathian region. *Science*. 290(5498), 1910-1917.